Time-Domain Universal Linear-Optical Operations for Universal Quantum Information Processing

Kazuma Yonezu, Yutaro Enomoto, Takato Yoshida, and Shuntaro Takeda*
Department of Applied Physics, School of Engineering, The University of Tokyo, 7-3-1 Hongo, Bunkyo-ku, Tokyo 113-8656, Japan

(Received 27 December 2022; accepted 23 June 2023; published 25 July 2023)

We demonstrate universal and programmable three-mode linear-optical operations in the time domain by realizing a scalable dual-loop optical circuit suitable for universal quantum information processing (QIP). The programmability, validity, and deterministic operation of our circuit are demonstrated by performing nine different three-mode operations on squeezed-state pulses, fully characterizing the outputs with variable measurements, and confirming their entanglement. Our circuit can be scaled up just by making the outer loop longer and also extended to universal quantum computers by incorporating feed forward systems. Thus, our work paves the way to large-scale universal optical QIP.

DOI: 10.1103/PhysRevLett.131.040601

Optics has been crucial in implementing various quantum information processing (QIP), such as quantum computing [1,2], quantum networking [3], and quantum simulation [4]. A core technology for universal optical QIP in both qubits and continuous variables is linear-optical operations, which linearly transform creation operators of photons [5]. Such operations are implementable only with linear optics and can create entanglement between optical modes [6], thereby providing core processing functions. These functions realize universal QIP, namely, an arbitrary unitary operation for either continuous-variable or qubit schemes, when combined with appropriate quantum light sources, detectors, and feed forward systems [1,2]. Even without the feed forward, linear-optical operations allow for implementing nonuniversal QIP, such as boson sampling [7,8] and quantum walk [9,10].

Much effort has been devoted to scaling up universal linear-optical operations toward large-scale universal quantum processors. Thus far, universal linear-optical operations have been implemented up to 20 modes by developing multimode linear interferometers on programmable photonic chips [11–14]. In such implementations, one optical path represents one mode, and spatial arrays of phase shifters (PSs) and beam splitters (BSs) perform the desired operations. In this path encoding, increasing the number of modes requires quadratically growing numbers of BSs and PSs. This makes the interferometer larger and makes the stabilization, calibration, and control of all the interferometric points more difficult, possibly limiting scalability.

A more scalable option to realize large-scale linear-optical operations is to use temporal encoding, where a large number of modes can be defined as sequential optical pulses on a single optical path [2]. High scalability of the temporal encoding has already been shown in recent optical demonstrations of quantum supremacy [15], scalable entanglement generation [16–19], and multimode multistep quantum gates [20–22]. The temporal encoding is also advantageous for scaling up universal linear-optical operations by adopting a dual-loop optical circuit proposed in Ref. [23]. Moreover, such a dual-loop architecture is extendable to universal QIP by appropriately incorporating feed forward systems [24,25]. Thus far, such architectures have been partly adopted to scale up specific nonuniversal QIP tasks, such as boson sampling [8] and quantum walk [10]. However, these experiments were designed for specific sampling tasks and are insufficient for universal QIP. More specifically, the linear-optical operations in these experiments were not universal due to the lack of complete dynamic controllability of the loops. Moreover, the loops were not phase stabilized, eliminating the coherence between optical pulses inside and outside the loops. In addition, these experiments only postselect the output to evaluate the sampling tasks and did not confirm the deterministic operation of even the most basic function (e.g., entanglement generation) of the linear-optical operations for universal QIP.

Here, we demonstrate universal and programmable three-mode linear-optical operations in the time domain by realizing a scalable dual-loop optical circuit suitable for universal QIP. Our dual-loop circuit achieves universal linear-optical operations by completing all the functionalities in the original proposal [23], including a variable beam splitter (VBS), a variable phase shifter (VPS), and fully phase-stabilized dual loops. We evaluate the performance of our circuit by using a squeezed light source and a homodyne detector with a programmable measurement basis. The programmability, validity, and deterministic operation of our circuit are demonstrated by performing

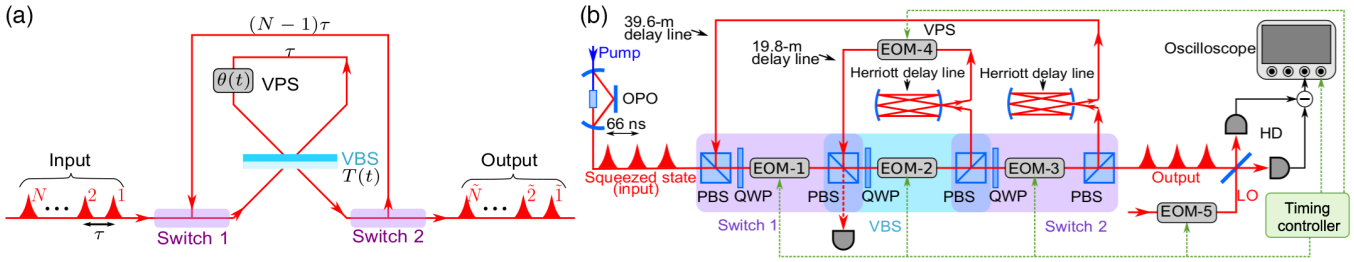

FIG. 1. Dual-loop circuit for universal linear-optical operations in the temporal encoding. (a) Conceptual schematic. (b) Experimental setup. See text for details. OPO, optical parametric oscillator; PBS, polarizing beam splitter; QWP, quarter-wave plate; EOM, electro-optic modulator; LO, local oscillator.

nine different three-mode operations on squeezed-state pulses, fully characterizing their output states via homodyne detection, and confirming their entanglement. These results together show the applicability of our circuit to arbitrary input states in both qubit and continuous-variable regimes, leading to universal QIP. In fact, the extension of our circuit to a universal quantum processor is straightforwardly possible by incorporating the feed forward system already realized in the previous work [22]. Note that our circuit is designed for various QIP and can process externally injected input states and export the output states; the previously demonstrated one-way quantum computing circuit [21] was designed for computational purposes and internally prepared input states and returned only calculation results instead of output quantum states. Furthermore, our dual-loop circuit can be straightforwardly scaled up just by making the outer loop longer and storing more modes in the loop. Thus, our work paves the way to large-scale universal QIP in the time domain.

Working principle of the dual-loop circuit.—In the typical path encoding, universal N-mode linear-optical operations can be performed by spatial arrays of BSs and PSs [26]. In the temporal encoding, the same operations can be done by the dual-loop circuit in Fig. 1(a) [23]. The working principle of the dual-loop circuit is as follows. First, N sequential pulsed optical modes with time interval τ are injected and stored in the dual-loop circuit via optical switches (switches 1, 2). Here, $N-1$ modes are stored in the outer loop whose round-trip time is $(N-1)\tau$, while the remaining mode is stored in the inner loop whose round-trip time is τ. The inner loop includes a VBS with transmissivity $T(t)$ and a VPS with phase $\theta(t)$, where t denotes time. This inner loop repeatedly performs two-mode BS interactions between the pulsed modes in the inner and outer loops while dynamically changing $T(t)$ and $\theta(t)$ for each pulse. It can be shown that such operations enable an arbitrary linear-optical operation between the N modes [27]. After the desired operations, switch 2 sequentially exports the output modes. This dual-loop circuit is highly scalable since it can process an arbitrary number of modes with a constant number of optical components, just by making the outer loop appropriately long. Furthermore, operations are fully programmable since they are determined by the electric control sequence of $T(t)$ and $\theta(t)$.

Figure 2 exemplifies a more concrete sequence to perform an arbitrary linear-optical operation for $N=3$ modes, which we adopt in our experiment. Figure 2(a) illustrates one of the possible configurations to perform an arbitrary three-mode linear-optical operation in the path encoding. The same operation can be done in the dual-loop

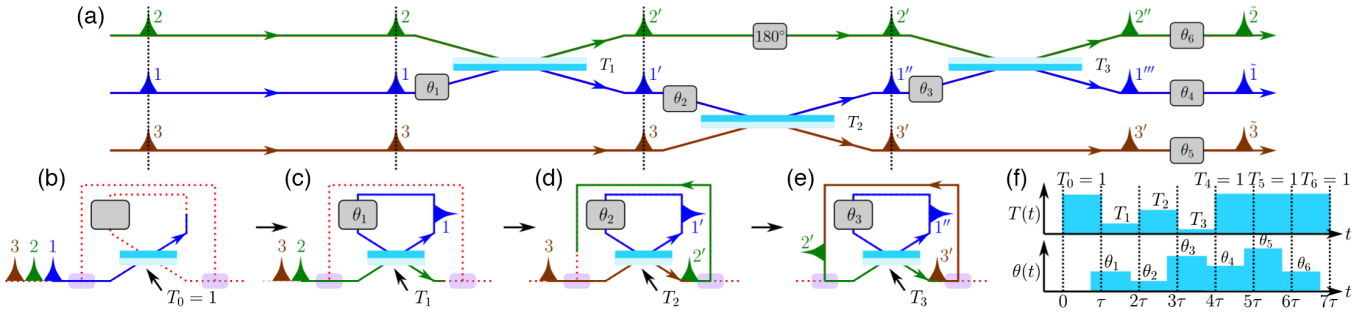

FIG. 2. Dynamics of the dual-loop circuit for universal three-mode linear-optical operations. (a) One of the possible configurations to perform universal three-mode linear-optical operations in the path encoding. The sides of the BSs that invert the phase of the reflected modes are colored light blue. A phase shift of 180° is added to make the circuit completely equivalent to our dual-loop circuit [27]. (b)–(e) Dynamics of the dual-loop circuit to perform universal three-mode operations in the temporal encoding. Subsequently, the transmissivity of the VBS is kept at 1 and the VPS adds phase shift θ_4, θ_5, and θ_6 to each mode. (f) Temporal control sequence for the dual-loop circuit.

circuit as shown in Figs. 2(b)–2(e) based on the control sequence in Fig. 2(f). A more general procedure to perform N-mode linear-optical operations is shown in the Supplemental Material [27].

Experimental setup.—We develop the dual-loop circuit with $N = 3$ that can perform universal and programmable three-mode linear-optical quantum operations, as shown in Fig. 1(b) [27]. Our setup achieves all the functionalities in the original proposal of the dual-loop circuit [23]. In our setup, we choose the time interval of $\tau = 66$ ns and the corresponding inner and outer loop lengths of 19.8 m (τ) and 39.6 m [$(N-1)\tau$], respectively. Both the inner and outer loops are phase locked. Two switches, one VPS and one VBS, are incorporated in the loops and synchronously controlled every $\tau = 66$ ns. The adjustable range of VPS phase shift and VBS transmissivity covers the entire range required for universality from 0 to 2π and from 0 to 1, respectively. To evaluate the performance of the operations in the dual-loop circuit, three-mode squeezed-state pulses are injected and each output pulse is measured by a

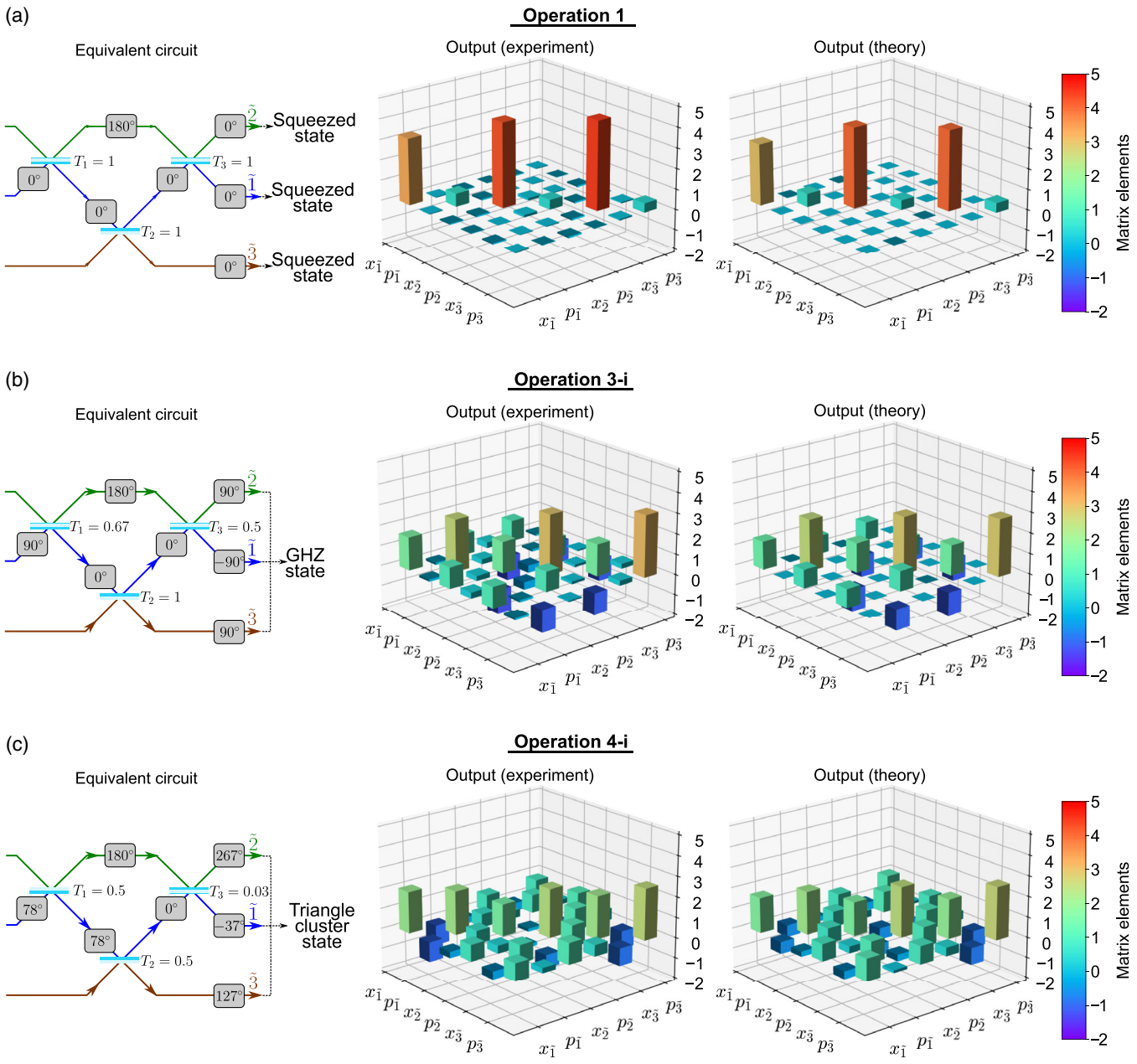

FIG. 3. Representative results of three-mode linear operations in the dual-loop circuit: (a) operation 1, (b) operation 3-i, (c) operation 4-i. The matrix elements represent covariances $\langle\hat{\xi}_i\hat{\xi}_j+\hat{\xi}_j\hat{\xi}_i\rangle/2-\langle\hat{\xi}_i\rangle\langle\hat{\xi}_j\rangle$, where $\langle\cdots\rangle$ denotes the mean value and $\hat{\xi} = (\hat{x}_{\tilde{1}}, \hat{p}_{\tilde{1}}, \hat{x}_{\tilde{2}}, \hat{p}_{\tilde{2}}, \hat{x}_{\tilde{3}}, \hat{p}_{\tilde{3}})^T$. The vacuum variance is set to 1 ($\hbar = 2$). Note that the phase-inverting side of one of the three BSs is flipped in (c), since the phase-inverting side of the VBS is flipped when $T < 0.5$ [17]. See text for details of each column.

homodyne detector (HD) with a variable measurement basis $\hat{x}\cos\phi(t) + \hat{p}\sin\phi(t)$, where $\hat{x}$ and $\hat{p}$ are the quadrature operators of the light field and ϕ is called a homodyne angle. Our control sequence is based on Figs. 2(b)–2(f), but the final unimportant local phase shifts $(\theta_4, \theta_5, \theta_6)$ in the VPS are omitted and equivalently performed by shifting the measurement bases at the HD. This reduces the number of round-trips of optical pulses in the loops and thus minimizes the optical loss during the operations.

Experimental results.—As a demonstration of programmable multimode linear-optical operations in the time domain, we perform nine different three-mode operations on the input p-squeezed-state pulses using our dual-loop circuit. It is known that appropriate linear operations can transform such squeezed states into various multimode continuous-variable entangled states [6,17]. Thus, our overall system can also be regarded as a general multimode continuous-variable photonic entanglement synthesizer [17]. We mainly adopt such operations for the demonstration and quantitatively evaluate the covariance matrices of the output states to verify the validity of the operations. Note that the covariance matrices fully characterize the output states, which are always Gaussian states with zero-mean quadratures in this experiment. In addition, we evaluate the degree of entanglement of the generated entangled states to show that the operations are performed in the quantum regime.

As shown in Fig. 2, three-mode linear operations are composed of three two-mode BS interactions. First, we run our dual-loop circuit in the simplest setting, where all these BS interactions are switched off by always setting the VBS transmissivity to 1 (operation 1). The equivalent circuit in the path encoding is shown in the left panel of Fig. 3(a). This operation only rearranges the order of the input modes and thus each output mode becomes a p-squeezed state. The experimental output covariance matrix is shown in the middle panel of Fig. 3(a). As expected, it shows (anti) squeezed variances in the p (x) quadratures for all modes, while not showing correlation between these modes. The theoretical covariance matrix including estimated optical losses [27] is also plotted in the right panel of Fig. 3(a), which reasonably well agrees with the experimental one. As can be seen from the covariance matrix, the output modes are slightly asymmetric. This is because, in our sequence, the squeezed state coming to mode $\tilde{1}$ suffers from an extra round-trip loss in the outer loop compared to the other modes.

Next, we perform three-mode linear-optical operations that generate various continuous-variable entangled states. In particular, we choose eight different operations and generate four types of entangled states: Einstein-Podolsky-Rosen (EPR) states [28] generated by switching on one BS interaction (operations 2-i, ii, iii), Greenberger-Horne-Zeilinger (GHZ) states [29] generated by switching on two BS interactions (operations 3-i, ii, iii), and two shapes of cluster states [30] generated by switching on all three BS interactions (operations 4-i, ii). Figures 3(b) and 3(c) are the representative results for operations 3 and 4, showing the equivalent path-encoding circuits and the output covariance

TABLE I. Fidelities and inseparability parameters for the output modes of various three-mode linear operations. See text for details.

Operation	Output state	Fidelity (I)	Fidelity (II)	Inseparability parameter
1	Individual squeezed vacuum states ($\tilde{1}$, $\tilde{2}$, and $\tilde{3}$)	0.992 ± 0.002	0.949 ± 0.003	
2-i	EPR state ($\tilde{1}$ and $\tilde{3}$), Squeezed vacuum state ($\tilde{2}$)	0.958 ± 0.007	0.894 ± 0.006	$\langle[\Delta(\hat{x}_{\tilde{1}} - \hat{x}_{\tilde{3}})]^2\rangle + \langle[\Delta(\hat{p}_{\tilde{1}} + \hat{p}_{\tilde{3}})]^2\rangle = 2.38 \pm 0.05$
2-ii	EPR state ($\tilde{2}$ and $\tilde{3}$), squeezed vacuum state ($\tilde{1}$)	0.966 ± 0.008	0.907 ± 0.008	$\langle[\Delta(\hat{x}_{\tilde{2}} - \hat{x}_{\tilde{3}})]^2\rangle + \langle[\Delta(\hat{p}_{\tilde{2}} + \hat{p}_{\tilde{3}})]^2\rangle = 2.09 \pm 0.03$
2-iii	EPR state ($\tilde{1}$ and $\tilde{2}$), squeezed vacuum state ($\tilde{3}$)	0.965 ± 0.004	0.896 ± 0.005	$\langle[\Delta(\hat{x}_{\tilde{1}} - \hat{x}_{\tilde{2}})]^2\rangle + \langle[\Delta(\hat{p}_{\tilde{1}} + \hat{p}_{\tilde{2}})]^2\rangle = 2.56 \pm 0.03$
3-i	GHZ state ($\tilde{1}$, $\tilde{2}$, and $\tilde{3}$)	0.947 ± 0.012	0.896 ± 0.009	$\langle[\Delta(\hat{x}_{\tilde{1}} - \hat{x}_{\tilde{2}})]^2\rangle + \langle[\Delta(\hat{p}_{\tilde{1}} + \hat{p}_{\tilde{2}} + \hat{p}_{\tilde{3}})]^2\rangle = 2.91 \pm 0.06$ $\langle[\Delta(\hat{x}_{\tilde{2}} - \hat{x}_{\tilde{3}})]^2\rangle + \langle[\Delta(\hat{p}_{\tilde{1}} + \hat{p}_{\tilde{2}} + \hat{p}_{\tilde{3}})]^2\rangle = 2.89 \pm 0.06$
3-ii	GHZ state ($\tilde{1}$, $\tilde{2}$, and $\tilde{3}$)	0.896 ± 0.007	0.816 ± 0.006	$\langle[\Delta(\hat{x}_{\tilde{1}} - \hat{x}_{\tilde{2}})]^2\rangle + \langle[\Delta(\hat{p}_{\tilde{1}} + \hat{p}_{\tilde{2}} + \hat{p}_{\tilde{3}})]^2\rangle = 3.39 \pm 0.04$ $\langle[\Delta(\hat{x}_{\tilde{2}} - \hat{x}_{\tilde{3}})]^2\rangle + \langle[\Delta(\hat{p}_{\tilde{1}} + \hat{p}_{\tilde{2}} + \hat{p}_{\tilde{3}})]^2\rangle = 3.09 \pm 0.04$
3-iii	GHZ state ($\tilde{1}$, $\tilde{2}$, and $\tilde{3}$)	0.888 ± 0.008	0.826 ± 0.007	$\langle[\Delta(\hat{x}_{\tilde{1}} - \hat{x}_{\tilde{2}})]^2\rangle + \langle[\Delta(\hat{p}_{\tilde{1}} + \hat{p}_{\tilde{2}} + \hat{p}_{\tilde{3}})]^2\rangle = 3.29 \pm 0.05$ $\langle[\Delta(\hat{x}_{\tilde{2}} - \hat{x}_{\tilde{3}})]^2\rangle + \langle[\Delta(\hat{p}_{\tilde{1}} + \hat{p}_{\tilde{2}} + \hat{p}_{\tilde{3}})]^2\rangle = 3.24 \pm 0.07$
4-i	Triangle cluster state ($\tilde{1}$, $\tilde{2}$, and $\tilde{3}$)	0.909 ± 0.019	0.863 ± 0.015	$\langle[\Delta(\hat{p}_{\tilde{1}} - \hat{x}_{\tilde{2}} - \hat{x}_{\tilde{3}})]^2\rangle + \langle[\Delta(\hat{p}_{\tilde{3}} - \hat{x}_{\tilde{1}} - \hat{x}_{\tilde{2}})]^2\rangle = 3.21 \pm 0.05$ $\langle[\Delta(\hat{p}_{\tilde{2}} - \hat{x}_{\tilde{1}} - \hat{x}_{\tilde{3}})]^2\rangle + \langle[\Delta(\hat{p}_{\tilde{3}} - \hat{x}_{\tilde{1}} - \hat{x}_{\tilde{2}})]^2\rangle = 3.80 \pm 0.04$
4-ii	Linear cluster state ($\tilde{1}$, $\tilde{2}$, and $\tilde{3}$)	0.976 ± 0.007	0.920 ± 0.008	$\langle[\Delta(\hat{p}_{\tilde{1}} - \hat{x}_{\tilde{3}})]^2\rangle + \langle[\Delta(\hat{p}_{\tilde{3}} - \hat{x}_{\tilde{1}} - \hat{x}_{\tilde{2}})]^2\rangle = 2.77 \pm 0.05$ $\langle[\Delta(\hat{p}_{\tilde{2}} - \hat{x}_{\tilde{3}})]^2\rangle + \langle[\Delta(\hat{p}_{\tilde{3}} - \hat{x}_{\tilde{1}} - \hat{x}_{\tilde{2}})]^2\rangle = 2.75 \pm 0.04$

matrices. As opposed to operation 1, the experimental covariance matrices show nonzero off-diagonal elements for all cases, which implies that some of the modes are entangled. In addition, the experimental covariance matrices agree well with the theoretical ones, demonstrating that the dual-loop circuit performs the three-mode operations as expected. The covariance matrices of all the other operations are summarized in the Supplemental Material [27].

Finally, we quantitatively evaluate the performance of all the above nine operations. We calculate and summarize the fidelities [fidelity (I)] between the experimental output quantum states and the theoretical ones including losses in Table I. All the operations show reasonably high fidelities of ∼0.9 or above. The deviations between the experimental and theoretical results can be attributed to the unwanted phase drift or fluctuation in the loops, as well as the deviation between the estimated losses and the actual ones. Note that the fidelities [fidelity (II)] between the experimental output states and ideal theoretical ones without including loop losses are also summarized in Table I. We also assess inseparability parameters for the generated entangled states to quantify the degree of entanglement. For all the cases except for operation 1, the sufficient condition for full inseparability is that the inseparability parameter is below 4 ($\hbar = 2$) [31]. As summarized in Table I, all the measured inseparability parameters satisfy this condition, indicating that all these operations are properly performed in the quantum regime. Here the inseparability parameters are slightly worse than the corresponding values in our previous single-loop experiment [17], due to the additional loss introduced by the extra round-trip in the outer loop. Note that all these operations in our dual-loop circuit are performed without any changes to the hardware configuration. Thus, these results demonstrate the validity, programmability, and deterministic operation of our dual-loop circuit that is universal for three-mode linear-optical operations.

Discussion.—In conclusion, we developed a scalable dual-loop circuit with complete dynamic controllability to perform universal three-mode linear-optical operations in the time domain. We showed its applicability to universal QIP in the continuous-variable regime. Furthermore, since our circuit can deal with any input state including qubits, it is also applicable to the qubit regime. The number of processable modes can be scaled up by several orders of magnitude, either by using a kilometer-long optical fiber for a stable and longer outer loop with comparable losses or by using broader-bandwidth light sources and electronics to shorten the time interval of pulses [2]. Furthermore, our dual-loop circuit can be integrated with other quantum light sources pumped by either continuous-wave or pulsed lasers. This work is extendable to loop-based universal optical quantum computers by incorporating feed forward systems [24,25], and it is thus a crucial step toward large-scale universal optical QIP.

The authors thank Akira Furusawa for providing space for the experiment. This work was partly supported by JSPS KAKENHI Grants No. 20H01833 and No. 21K18593, MEXT Leading Initiative for Excellent Young Researchers, Toray Science Foundation (19-6006), and the Canon Foundation.

Note added.—We have recently become aware of a work [32] in which a loop circuit with a different configuration performed universal linear-optical operations in the time domain. However, in the same way as the previous works [8,10], this work was designed for a specific nonuniversal task (Gaussian boson sampling) and sampled the output at a fixed measurement basis without characterizing the operations themselves.

*takeda@ap.t.u-tokyo.ac.jp

[1] E. Knill, R. Laflamme, and G. J. Milburn, Nature (London) **409**, 46 (2001).
[2] S. Takeda and A. Furusawa, APL Photonics **4**, 060902 (2019).
[3] S. Wehner, D. Elkouss, and R. Hanson, Science **362**, eaam9288 (2018).
[4] F. Flamini, N. Spagnolo, and F. Sciarrino, Rep. Prog. Phys. **82**, 016001 (2018).
[5] P. Kok, W. J. Munro, K. Nemoto, T. C. Ralph, J. P. Dowling, and G. J. Milburn, Rev. Mod. Phys. **79**, 135 (2007).
[6] P. van Loock, C. Weedbrook, and M. Gu, Phys. Rev. A **76**, 032321 (2007).
[7] S. Aaronson and A. Arkhipov, in *Proceedings of the Forty-Third Annual ACM Symposium on Theory of Computing* (Association for Computing Machinery, New York, 2011), pp. 333–342.
[8] Y. He, X. Ding, Z.-E. Su, H.-L. Huang, J. Qin, C. Wang, S. Unsleber, C. Chen, H. Wang, Y.-M. He *et al.*, Phys. Rev. Lett. **118**, 190501 (2017).
[9] Y. Aharonov, L. Davidovich, and N. Zagury, Phys. Rev. A **48**, 1687 (1993).
[10] A. Schreiber, A. Gábris, P. P. Rohde, K. Laiho, M. Štefaňák, V. Potoček, C. Hamilton, I. Jex, and C. Silberhorn, Science **336**, 55 (2012).
[11] J. Carolan, C. Harrold, C. Sparrow, E. Martín-López, N. J. Russell, J. W. Silverstone, P. J. Shadbolt, N. Matsuda, M. Oguma, M. Itoh *et al.*, Science **349**, 711 (2015).
[12] X. Qiang, X. Zhou, J. Wang, C. M. Wilkes, T. Loke, S. O'Gara, L. Kling, G. D. Marshall, R. Santagati, T. C. Ralph *et al.*, Nat. Photonics **12**, 534 (2018).
[13] C. Taballione, M. C. Anguita, M. de Goede, P. Venderbosch, B. Kassenberg, H. Snijders, D. Smith, J. P. Epping, R. van der Meer, P. W. Pinkse *et al.*, arXiv:2203.01801.
[14] C. Taballione, R. van der Meer, H. J. Snijders, P. Hooijschuur, J. P. Epping, M. de Goede, B. Kassenberg, P. Venderbosch, C. Toebes, H. van den Vlekkert *et al.*, Mater. Quantum Technol. **1**, 035002 (2021).
[15] L. S. Madsen, F. Laudenbach, M. F. Askarani, F. Rortais, T. Vincent, J. F. Bulmer, F. M. Miatto, L. Neuhaus, L. G. Helt, M. J. Collins *et al.*, Nature (London) **606**, 75 (2022).

[16] S. Yokoyama, R. Ukai, S. C. Armstrong, C. Sornphiphatphong, T. Kaji, S. Suzuki, J. Yoshikawa, H. Yonezawa, N. C. Menicucci, and A. Furusawa, Nat. Photonics **7**, 982 (2013).
[17] S. Takeda, K. Takase, and A. Furusawa, Sci. Adv. **5**, eaaw4530 (2019).
[18] E. Meyer-Scott, N. Prasannan, I. Dhand, C. Eigner, V. Quiring, S. Barkhofen, B. Brecht, M. B. Plenio, and C. Silberhorn, Phys. Rev. Lett. **129**, 150501 (2022).
[19] D. Istrati, Y. Pilnyak, J. Loredo, C. Antón, N. Somaschi, P. Hilaire, H. Ollivier, M. Esmann, L. Cohen, L. Vidro *et al.*, Nat. Commun. **11**, 5501 (2020).
[20] W. Asavanant, B. Charoensombutamon, S. Yokoyama, T. Ebihara, T. Nakamura, R. N. Alexander, M. Endo, J. Yoshikawa, N. C. Menicucci, H. Yonezawa *et al.*, Phys. Rev. Appl. **16**, 034005 (2021).
[21] M. V. Larsen, X. Guo, C. R. Breum, J. S. Neergaard-Nielsen, and U. L. Andersen, Nat. Phys. **17**, 1018 (2021).
[22] Y. Enomoto, K. Yonezu, Y. Mitsuhashi, K. Takase, and S. Takeda, Sci. Adv. **7**, eabj6624 (2021).
[23] K. R. Motes, A. Gilchrist, J. P. Dowling, and P. P. Rohde, Phys. Rev. Lett. **113**, 120501 (2014).
[24] P. P. Rohde, Phys. Rev. A **91**, 012306 (2015).
[25] S. Takeda and A. Furusawa, Phys. Rev. Lett. **119**, 120504 (2017).
[26] M. Reck, A. Zeilinger, H. J. Bernstein, and P. Bertani, Phys. Rev. Lett. **73**, 58 (1994).
[27] See Supplemental Material at http://link.aps.org/supplemental/10.1103/PhysRevLett.131.040601 for further details on experimental methods, theoretical decomposition of linear operations, and supplemental experimental results, which also includes additional Refs. [33–42].
[28] Z. Y. Ou, S. F. Pereira, H. J. Kimble, and K. C. Peng, Phys. Rev. Lett. **68**, 3663 (1992).
[29] T. Aoki, N. Takei, H. Yonezawa, K. Wakui, T. Hiraoka, A. Furusawa, and P. van Loock, Phys. Rev. Lett. **91**, 080404 (2003).
[30] X. Su, A. Tan, X. Jia, J. Zhang, C. Xie, and K. Peng, Phys. Rev. Lett. **98**, 070502 (2007).
[31] P. van Loock and A. Furusawa, Phys. Rev. A **67**, 052315 (2003).
[32] S. Yu, Z.-P. Zhong, Y. Fang, R. B. Patel, Q.-P. Li, W. Liu, Z. Li, L. Xu, S. Sagona-Stophel, E. Mer *et al.*, arXiv:2210.14877.
[33] D. Herriott, H. Kogelnik, and R. Kompfner, Appl. Opt. **3**, 523 (1964).
[34] J. Yoshikawa, S. Yokoyama, T. Kaji, C. Sornphiphatphong, Y. Shiozawa, K. Makino, and A. Furusawa, APL Photonics **1**, 060801 (2016).
[35] E. D. Black, Am. J. Phys. **69**, 79 (2001).
[36] K. Fukui, A. Tomita, A. Okamoto, and K. Fujii, Phys. Rev. X **8**, 021054 (2018).
[37] K. R. Motes, J. P. Dowling, A. Gilchrist, and P. P. Rohde, Phys. Rev. A **92**, 052319 (2015).
[38] H. Wang, W. Li, X. Jiang, Y.-M. He, Y.-H. Li, X. Ding, M.-C. Chen, J. Qin, C.-Z. Peng, C. Schneider *et al.*, Phys. Rev. Lett. **120**, 230502 (2018).
[39] R. Simon, N. Mukunda, and B. Dutta, Phys. Rev. A **49**, 1567 (1994).
[40] G. B. Folland, in *Harmonic Analysis in Phase Space (AM-122)*, Volume 122 (Princeton University Press, Princeton, NJ, 2016).
[41] H. de Guise, O. Di Matteo, and L. L. Sánchez-Soto, Phys. Rev. A **97**, 022328 (2018).
[42] W. R. Clements, P. C. Humphreys, B. J. Metcalf, W. S. Kolthammer, and I. A. Walmsley, Optica **3**, 1460 (2016).